J. Electrochem. Sci. Eng. **16** (2026) 3245; https://doi.org/10.5599/jese.3245

Open Access : : ISSN 1847-9286
https://pub.iapchem.org/ojs/index.php/JESE

Original scientific paper

Electroless cobalt coating of BNi-2 powders: process development and characterization

Tansu Göynük[1,2,✉] and İshak Karakaya[1]

[1]*Department of Metallurgical and Materials Engineering, Middle East Technical University, 06800, Ankara, Türkiye*
[2]*ROKETSAN Inc., P.K. 30 Elmadağ 06780 Ankara, Turkey*

Corresponding Authors: ✉*e181820@metu.edu.tr*; Tel.: +90-312-860-55-00-7254

Received: February 6, 2026; Revised: May 9, 2026; Published: May 14, 2026

Abstract

Electroless cobalt deposition and examination of how cobalt enrichment on the particle surface modifies the chemical composition and thermal behaviour of the commercial BNi-2 brazing alloy powder was investigated in this study. A multi-step surface preparation sequence involving oxide removal, Sn-based sensitization, and Pd activation was employed prior to cobalt deposition in an alkaline $CoSO_4$-NaH_2PO_2 bath. A design of experiments approach was used to evaluate the influence of plating temperature, cobalt sulphate concentration, hypophosphite concentration, and coating time on cobalt uptake. ICP-OES analyses showed that cobalt incorporation increased from 1.1 to 7.0 wt.% across the selected parameter range. Differential scanning calorimetry revealed that coating levels up to 7 wt.% Co elevate the solidus temperature, while decreasing the liquidus temperature, resulting in a narrower melting interval. Thermodynamic simulations confirmed these trends, showing suppression of borides and enhanced γ/γ' stability where γ denotes the Ni-rich face-cantered cubic matrix phase and γ' represents the ordered $Ni_3(Al,Ti)$-type strengthening phase with increasing cobalt content. EDS mapping of coated powder showed continuous cobalt distribution at the particle perimeter. Overall, the results provided a quantitative basis for linking coating parameters to cobalt incorporation and corresponding modifications in melting behaviour.

Keywords

Ni-based braze alloy; brazing powder modification; cobalt plating; plating experimental design; coated powder

Introduction

Ni-based brazing filler metals are widely used to join heat-resistant alloys in aero-engine and power-generation components, where joints must withstand high temperatures, mechanical loads

and corrosive environments over long service lives [1-3]. Among the commercial alloys, BNi-2 (Ni-Cr-Fe-B-Si) is particularly attractive because of its relatively low melting range, governed by boron and silicon as melting-point depressants, which allows vacuum brazing of complex assemblies without excessive grain growth or distortion of the base materials [4-6]. This filler has been successfully employed for joining nickel-based superalloys such as Inconel 718 and related alloys, as well as in dissimilar configurations where high wetting ability and good capillary flow are required [4,7,8]. In parallel, titanium alloys like Ti-6Al-4V and Ni-based superalloys such as Inconel 718 remain key structural materials for hot-section components, and several recent studies have highlighted the narrow processing window for brazing and transient-liquid-phase (TLP) bonding of Ti-6Al-4V/Inconel 718 and Ti-6Al-4V/steel joints when BNi-2 was used as the filler [7-9]. The beneficially low brazing temperature of BNi-2 is achieved by relatively high additions of B and Si, but these elements promote the formation of hard, brittle borides and silicides in the joint, and can limit high-temperature strength and fatigue performance if they solidify as continuous intermetallic networks [8-10].

Numerous works on Ni-B-Si brazes and diffusion-brazed joints have shown that controlling boron and silicon activity, as well as their partitioning into phases such as Ni_3B, CrB or complex Ni-Si-B compounds, is critical for balancing fluidity, joint soundness and re-melt behaviour [10-12]. For Ti- and Ni-based superalloy joints, this issue is even more acute, because any reduction in joint solidus temperature or persistence of low-melting eutectics can compromise service at temperatures approaching 900 to 1000 °C [11,12]. Consequently, there has been sustained interest in strategies that either raise the effective solidus of Ni-based brazing alloys or limit the volume fraction and connectivity of brittle MPD (melting point depressant)-rich phases, without sacrificing wetting and processability.

One straightforward route is bulk compositional redesign of the filler. Approaches include reducing B or Si, introducing elements such as Nb, Mo or refractory additions to stabilize higher-melting solid solutions, or moving towards multi-principal-element Ni-based braze alloys with narrower melting intervals [13, 14]. Such fillers can indeed provide higher joint solidus and improved creep resistance, but they typically require new alloy development, atomization and full process re-qualification, which is costly and time-consuming. In parallel, process-based concepts such as TLP bonding or diffusion brazing seek to raise the joint re-melt temperature by driving isothermal solidification and homogenization, so that the final microstructure approaches that of the base alloy [15,16]. While highly effective, TLP routes often demand long holds at elevated temperatures and precise control of interlayer thickness and chemistry, which may not be compatible with all component geometries or production environments.

Surface-engineering of existing commercial fillers offers an alternative path to tune melting behaviour and interfacial reactions without altering the bulk powder chemistry. Electroless plating is a mature technology capable of depositing conformal metallic coatings, such as Ni, Co or Ni-P, on complex three-dimensional substrates, including ceramic and metallic powders, with high thickness uniformity. Studies on electroless Ni or Ni-P coatings on B_4C, $CaCO_3$ and Fe-Co powders have demonstrated that such coatings can substantially modify the thermal stability, densification behaviour and mechanical response of the resulting composites or sintered bodies, while maintaining good adhesion and coverage around individual particles [17-20]. In parallel, alloy design studies on mechanically alloyed Ni-based brazing powders have shown that direct Co and Cr additions increase the solidus temperature and refine powder morphology, indicating that cobalt is a promising element for tailoring the melting characteristics of Ni-based fillers [21]. However, the use of electroless cobalt deposition specifically on commercial BNi-2 powders, and the implications

of such a surface modification on powder chemistry and phase equilibria, have only recently begun to attract attention.

In previous studies, Göynük *et al*. applied electroless cobalt coatings to BNi-2 filler powder and investigated their effect on the vacuum brazing performance of Inconel 718 joints, reporting changes in melting behaviour, interfacial phase formation and joint mechanical properties compared with uncoated filler [22]. The electroless cobalt modification concept underlying this approach was also disclosed in a national patent application, establishing the basis of the surface engineering strategy employed in the present work [23]. The present study focuses specifically on the development and characterization of electroless cobalt-coated BNi-2 powders, decoupled from any brazing configuration. The work describes the surface conditioning and electroless Co deposition procedures applied to commercial BNi-2 powder, the use of a design-of-experiments approach to optimize bath chemistry and process parameters, and the subsequent microstructural and thermodynamic assessment of the coated powders by ICP-OES, DSC/JMatPro, SEM/EDS and XPS analyses. By concentrating on the powder-level metallurgy, this study aims to clarify how a cobalt-rich surface shell on BNi-2 particles influences global alloy chemistry, phase stability and melting characteristics, thereby providing a platform for future brazing studies in Ti- and Ni-based high-temperature alloy systems.

Experimental

Commercial BNi-2 nickel-based brazing alloy powder, with a d_{90} value of approximately 106 µm (meaning that 90 % of the particles are smaller than this size), supplied by Sentes-Bir A.Ş., was employed as the substrate material for the coating experiments. The powder was firstly cleaned through sequential acid and alkali immersion, *i.e.* it was immersed for 10 minutes in a 0.1 M nitric acid (HNO_3) bath to dissolve oxides and passive films, what is followed by a 10-minute treatment in 0.1 M sodium hydroxide (NaOH) solution to remove remaining organics. Powder was thoroughly rinsed with deionized water to remove residual species after each step and chemically activated through a sensitization-activation procedure after cleaning. Sensitization was carried out in a tin chloride ($SnCl_2{\cdot}2H_2O$)-hydrochloric acid (HCl) solution, allowing Sn^{2+} ions to adsorb onto the surfaces of the particles. The sensitized powder was then transferred into an activation bath containing palladium chloride ($PdCl_2$) and HCl, where catalytic Pd nuclei were formed *via* redox exchange between Pd^{2+} and Sn^{2+} ions. These nuclei acted as catalytic sites for subsequent cobalt reduction during electroless plating. To avoid particle clustering and ensure homogeneous treatment, each step was assisted by ultrasonic agitation. A schematic representation of the surface preparation and electroless cobalt deposition sequence for the BNi-2 powder is shown in Figure 1. The diagram outlines the sequential removal of surface oxides, sensitization with Sn^{2+} species, activation *via* Pd nucleation, and the subsequent autocatalytic reduction of Co^{2+} ions by hypophosphite during the electroless plating step. Each stage plays a specific role in establishing a clean and catalytically active surface that enables uniform cobalt nucleation and growth. Collectively, these steps ensure the formation of a continuous and conformal Co layer around BNi-2 particles.

The bath compositions and operational conditions [24] used for sensitization and activation are summarized in Table 1.

Table 1. *Summary of the sensitization and activation baths used for surface preparation of BNi-2 powder prior to electroless cobalt deposition, including chemical components, concentrations and operating conditions*

Step	Chemical components	Composition	Operating conditions
Sensitization	$SnCl_2{\cdot}2H_2O$ + HCl	20 g L^{-1} $SnCl_2{\cdot}2H_2O$ + 40 mL L^{-1} HCl	25 °C, 15 min, ultrasonicated
Activation	$PdCl_2$ + HCl	0.5 g L^{-1} $PdCl_2$ + 120 mL L^{-1} HCl	25 °C, 15 min, ultrasonicated

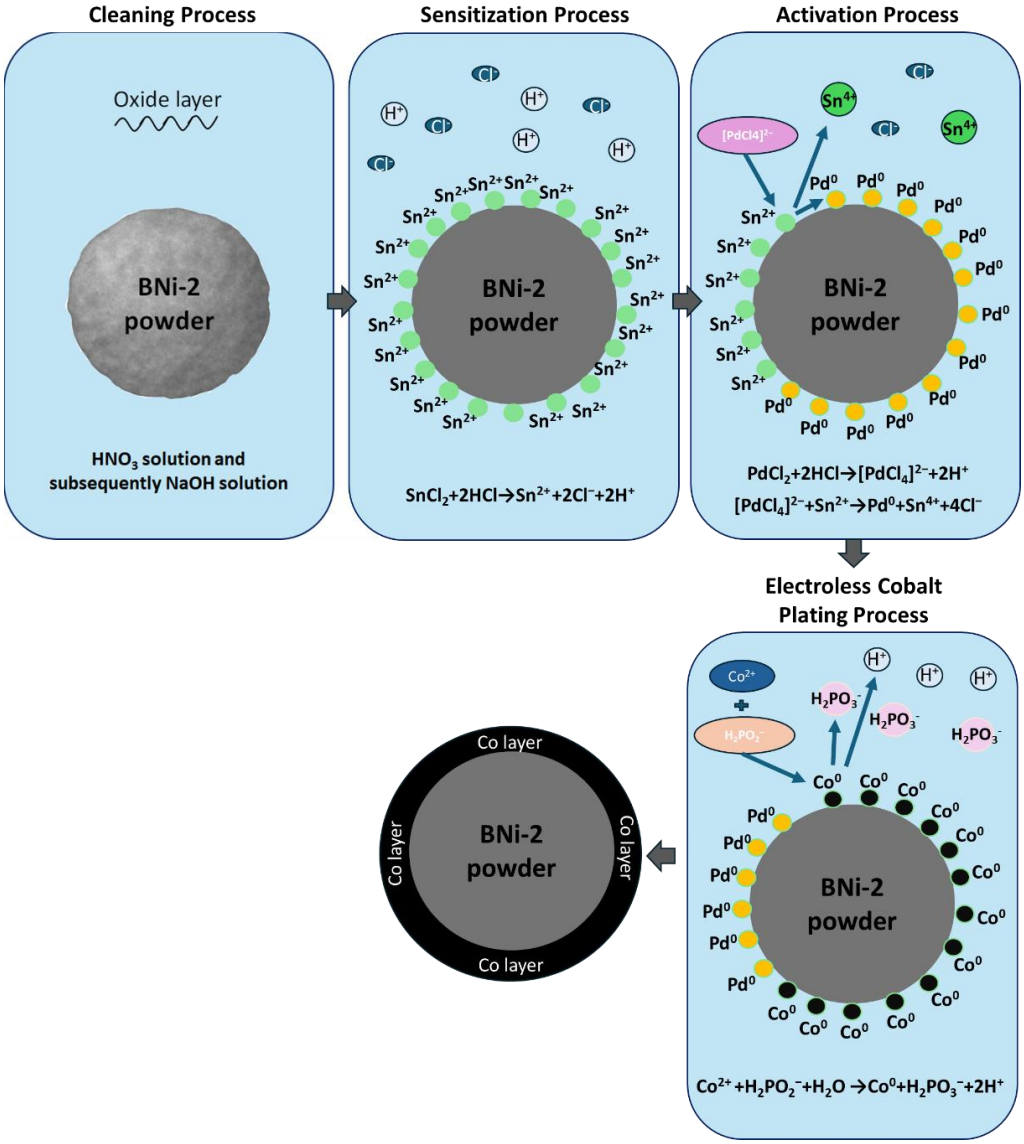

Figure 1. *Schematic illustration of the sequential surface preparation and electroless cobalt deposition steps applied to BNi-2 powder. The process includes oxide removal, Sn^{2+}-based sensitization, Pd activation through ionic exchange, and the autocatalytic reduction of Co^{2+} by hypophosphite during cobalt plating, resulting in the formation of a continuous cobalt-rich layer around the powder surface*

Following activation, the powder was subjected to electroless cobalt deposition in an alkaline plating bath. The main source of cobalt ions was cobalt sulphate heptahydrate ($CoSO_4 \cdot 7H_2O$). Sodium hypophosphite monohydrate ($NaH_2PO_2 \cdot H_2O$) acted as the reducing agent, while trisodium citrate dihydrate ($C_6H_5Na_3O_7 \cdot 2H_2O$) served as a complexing agent to stabilize the Co^{2+} ions in solution. Boric acid (H_3BO_3) was added as a buffer to maintain pH stability and minimize hydrogen evolution. The pH of the bath was adjusted and maintained between 9 and 11 using sodium hydroxide (NaOH). A stable alkaline environment is essential for controlling cobalt ion reduction kinetics and ensuring uniform deposition. The baseline bath composition and operating window were selected in reference to previous electroless cobalt studies [24], where an 8 min deposition time was employed. In the present work, this duration was taken as a central reference value, and plating time was systematically varied within the experimental design to evaluate its influence on cobalt incorporation. Upon completion, the powders were repeatedly rinsed with deionized water and oven-dried at 110 °C for 8 hours to remove residual moisture. The bath composition and operating parameters are presented in Table 2.

Table 2. *Composition and operating ranges of the electroless cobalt plating bath used for Co deposition on BNi-2 powder, listing the principal chemical species, their concentration intervals, and functional roles within the bath*

Component	Concentration range, g L^{-1}	Remarks / conditions
$CoSO_4 \cdot 7H_2O$	15 to 30	Metal ion source, pH 9-11
$NaH_2PO_2 \cdot H_2O$	20 to 50	Reducing agent
$C_6H_5Na_3O_7 \cdot 2H_2O$	15 to 30	Complexing agent
H_3BO_3	25	Buffer
$C_4H_4O_4$ (optional)	1.5	Additive for bath stability

To evaluate the effects of key process parameters on coating efficiency and cobalt deposition rate, a full factorial Design of Experiments (DoE) approach was implemented using Minitab [25]. Four variables were considered: plating temperature (three levels), cobalt sulphate concentration (three levels), sodium hypophosphite concentration (two levels), and plating time (two levels). This resulted in a 3×3×2×2 full-factorial matrix with 36 experimental runs. All coated powder batches obtained from these experiments were subjected to ICP-OES analysis to quantify cobalt incorporation. The selected parameter matrix is given in Table 3.

Table 3. *Experimental parameter levels used in the full factorial DoE study, showing the combinations of plating temperature, cobalt sulphate concentration, sodium hypophosphite concentration and coating time selected to evaluate their influence on cobalt deposition on BNi-2 powders*

Temperature, °C	$CoSO_4$ content, g L^{-1}	NaH_2PO_2 content, g L^{-1}	Plating time, min
60	20	20	5
80	25	35	10
-	30	50	-

Results and discussion

A total of 36 experimental conditions were evaluated within the full factorial design. To determine the actual cobalt content deposited on the powder surface after electroless coating, inductively coupled plasma-optical emission spectrometry (ICP-OES) analysis was carried out to these 36 coated powder samples. The analysis enabled the verification of cobalt incorporation efficiency as a function of the process parameters, including temperature, cobalt sulphate and sodium hypophosphite concentrations, and plating duration. Based on the ICP-OES results, cobalt incorporation ranged up to approximately 7 wt.%. For comparative microstructural and thermodynamic assessment, four representative cobalt coating levels (approximately 1, 3, 5, and 7 wt.% Co) were selected for detailed DSC and JMatPro analyses. Table 4 summarizes the experimental conditions and the elemental composition of the uncoated BNi-2 powders and the selected four coated samples. Nickel remains the base matrix element, while the progressive increase in cobalt content indicates the degree of surface modification achieved under different processing conditions.

The data reveal a clear dependence of cobalt deposition on the processing conditions. The cobalt content on the powder surface increased systematically with higher plating temperature, longer plating duration, and greater cobalt sulphate concentration in the bath. This trend indicates that elevated temperature and higher cobalt ion availability in the solution enhanced the reduction kinetics of Co^{2+} ions, leading to more complete coverage of the powder surface with metallic cobalt. Similarly, extended coating time yielded more deposition and greater surface enrichment. In contrast, increasing the concentration of sodium hypophosphite resulted in a decrease in the measured cobalt content. This behaviour can be attributed to the accelerated side reactions

associated with excessive hypophosphite, such as enhanced hydrogen gas evolution, which competes with the cobalt reduction reaction. Consequently, the effective deposition efficiency of Co decreased at higher NaH_2PO_2 levels.

Table 4. *ICP-OES results showing the elemental compositions of uncoated and electroless cobalt-coated BNi-2 powder. From the total 36 experimental runs of the full factorial design, powder corresponding to approximately 1, 3, 5 and 7 wt.% Co was selected as representative condition for detailed comparative analysis. The listed plating parameters (temperature, cobalt sulphate concentration, hypophosphite concentration, and coating time) correspond to these selected samples*

Experimental conditions				Content, wt.%									
Temp, °C	Concentration, g L^{-1}		Time, min										
	$CoSO_4$	NaH_2PO_2		Ni	Cr	B	Si	Fe	Ti	Al	Zr	Co	Pd
Uncoated BNi-2				Bal.	7.6	3.2	4.6	3.2	0.03	0.05	0.03	0.4	0.4
60	20	50	5	Bal.	7.6	3.1	4.5	3.2	0.04	0.04	0.03	1.1	0.5
60	20	35	5	Bal.	7.8	3.2	4.5	3.4	0.05	0.03	0.05	3.0	0.6
60	20	20	5	Bal.	7.6	3.3	4.6	3.5	0.03	0.04	0.04	5.0	0.2
80	30	20	10	Bal.	7.9	3.3	4.9	3.1	0.04	0.02	0.04	7.0	0.7

Based on the experimental design and regression analysis, the relationship between the coating parameters and the measured cobalt content was expressed using the empirical Equation (1):

$$W_{Co} = 3.25 + 0.05T + 0.17M_{CoSO_4} - 0.14M_{NaH_2PO_2} + 0.04t \quad (1)$$

where T / °C is plating temperature, M_{CoSO_4} / g L^{-1} is concentration of cobalt sulphate in the plating bath, $M_{NaH_2PO_2}$ / g L^{-1} is concentration of sodium hypophosphite in the plating bath, t / min is plating time and W_{Co} / wt.% is cobalt amount in the powder.

The regression model was derived from the complete 36-run dataset. This model was derived within the selected parameter ranges and represents the quantitative effect of each variable on cobalt incorporation. The positive coefficients of temperature, cobalt sulphate concentration, and plating time indicate that an increase in these parameters promotes higher cobalt deposition on the powder surface. Conversely, the negative coefficient of sodium hypophosphite concentration confirms its inhibitory influence on cobalt reduction, consistent with the experimental observations. The individual influence of each process parameter on cobalt incorporation is summarized in Figure 2. The first panel shows that higher bath temperature promotes cobalt deposition on the powder surface. The second panel indicates a gradual increase in cobalt content with increasing $CoSO_4$ concentration. In contrast, the third panel shows that a higher NaH_2PO_2 concentration reduces the deposited cobalt level. The fourth panel shows a moderate increase in cobalt incorporation with plating time within the investigated range. These trends provide a visual representation of the parameter effects that are later quantified by the regression model.

The thermal behaviour of the uncoated and cobalt-coated BNi-2 powder was investigated using differential scanning calorimetry (DSC), and the corresponding curves are presented in Figure 3. The DSC results revealed that the addition of cobalt gradually increased the solidus temperature of the BNi-2 alloy from 970 °C (uncoated) to 990 °C (7 wt.% Co). This shift indicates that cobalt addition promotes greater thermal stability of the alloy matrix, possibly through the formation of Co-Ni solid solutions that strengthen atomic bonding and retard the onset of melting. In contrast, the liquidus temperature decreased from 1050 to 1010 °C with increasing cobalt content. This behaviour suggests that cobalt incorporation promotes partial modification of the eutectic phase composition, facilitating earlier completion of melting.

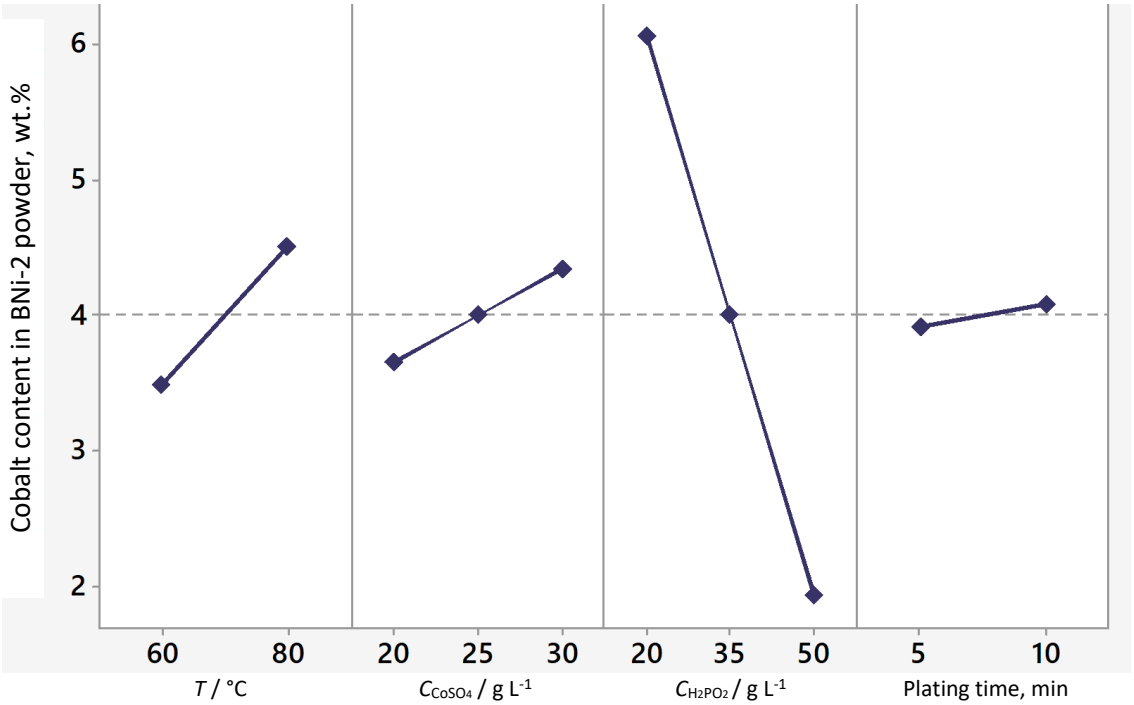

Figure 2. *Main effect plots obtained from the design-of-experiments analysis, illustrating the influence of plating temperature, $CoSO_4$ concentration, NaH_2PO_2 concentration, and coating time on the cobalt content incorporated into BNi-2 powder during electroless deposition. The y-axis represents the measured cobalt content determined by ICP-OES*

The resulting narrower melting range at higher Co levels (especially above 5 wt.%) is beneficial for brazing applications, as it can improve filler flow and wetting uniformity while reducing the likelihood of incomplete melting. Additionally, the endothermic peaks near 950 to 1000 °C in Figure 3 correspond to the primary melting event of the Ni-B-Si eutectic phase, while minor exothermic features around 500 to 700 °C are associated with crystallization or structural relaxation of the amorphous fraction.

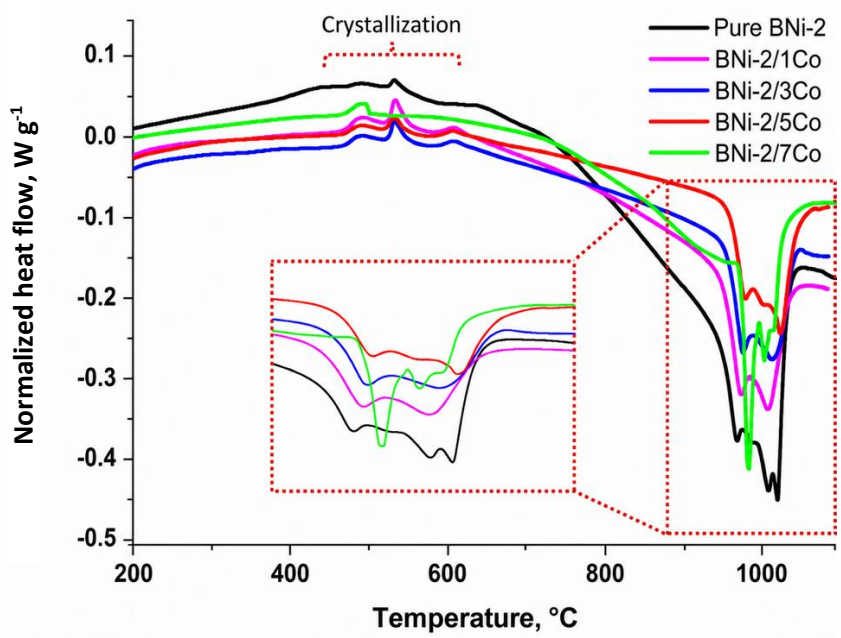

Figure 3. *Differential scanning calorimetry curves of uncoated and cobalt-coated BNi-2 powder, showing the influence of cobalt content on crystallization behavior and melting characteristics. Inset highlight the shifts in solidus and liquidus regions as cobalt incorporation increases from 1 to 7 wt.%*

These transformations appear slightly shifted with cobalt addition, further confirming that cobalt modifies the thermal response of the alloy. The DSC analysis indicates that cobalt addition to BNi-2 powder refines the melting characteristics, slightly raises the onset of melting, and reduces the total melting interval, which is an effect that is favourable for achieving controlled wetting and stable brazing behaviour in dissimilar alloy joining.

According to the JMatPro thermodynamic simulations [26], cobalt addition noticeably altered the phase stability of the BNi-2 alloy, as shown in Figure 4. In this context, γ refers to the Ni-rich face-centered cubic (FCC) solid solution matrix, while γ′ corresponds to the ordered intermetallic $Ni_3(Al,Ti)$-type phase that contributes to strengthening in Ni-based systems. In the pure BNi-2 condition, γ (Ni-rich matrix), MB_2, and M_3B_2 borides dominated the microstructure, while minor carbides such as M_7C_3 appeared at low fractions. As the temperature increased, these borides gradually dissolved, forming a liquid phase near 970 °C and completing melting at approximately 1050 °C. With cobalt addition, the fraction of γ phase increased while the boride phases were progressively suppressed, and secondary γ′ and $M_{23}C_6$ phases began to form between 400 and 800 °C. The 3 wt.% Co alloy showed a higher γ′ stability window and reduced MB_2 content, resulting in an upward shift of the solidus temperature and a slight decrease in the liquidus point. Increasing Co content to 5 wt.% further promoted the γ and γ′ fractions while minimizing brittle borides, leading to improved solid-phase strength retention at intermediate temperatures. At 7 wt.% Co, γ became the dominant phase across almost the entire solid range, and the γ′ fraction expanded significantly, indicating strong solute stabilization and solid-solution strengthening.

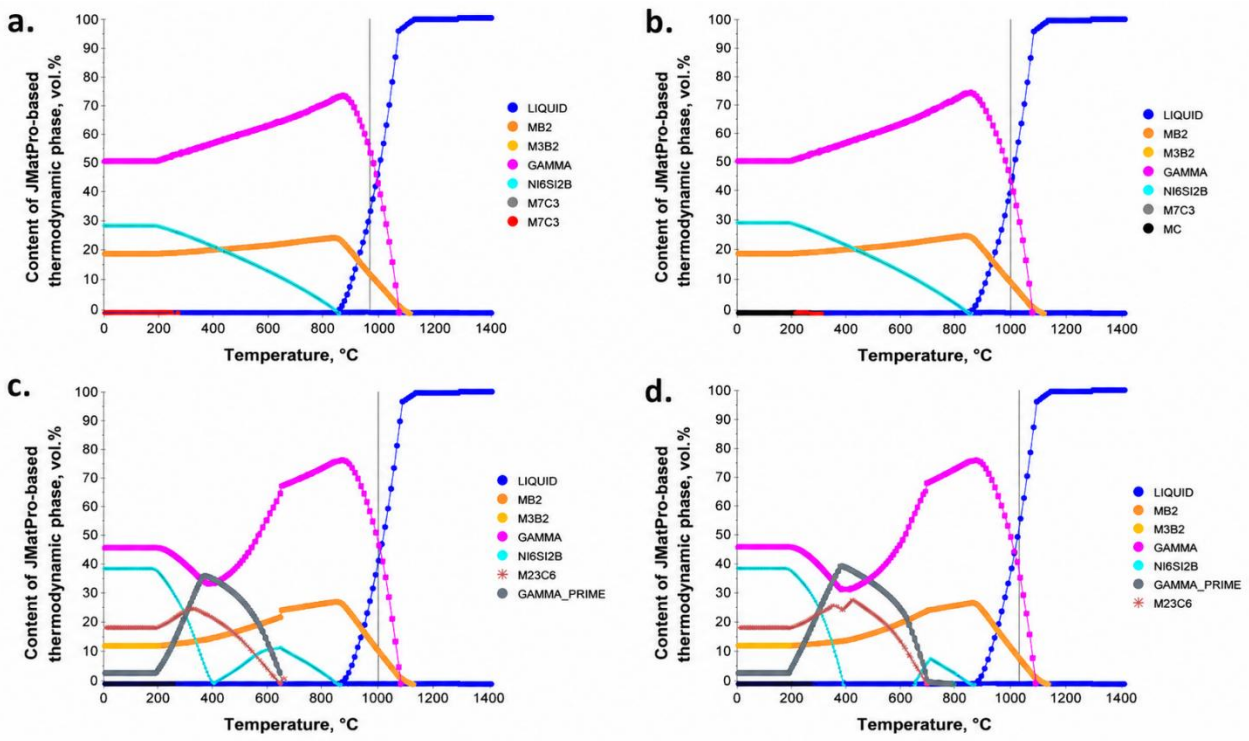

Figure 4. *JMatPro-based thermodynamic phase prediction curves for uncoated and cobalt-modified BNi-2 powder: (a) phase evolution of uncoated BNi-2; (b) phase evolution of 3 wt.% Co-coated BNi-2; (c) phase evolution of 5 wt.% Co-coated BNi-2; (d) phase evolution of 7 wt.% Co-coated BNi-2*

The simulated melting behaviour revealed that the solidus temperature continuously increased while the liquidus temperature decreased with higher Co levels, indicating a narrowing of the melting interval. These simulated values are consistent with DSC results, where the solidus shifted from 970 to 990 °C and the liquidus decreased from 1050 to 1010 °C, confirming the JMatPro

predictions. Overall, cobalt addition refines the phase constitution and adjusts the melting characteristics of BNi-2 in a manner fully coherent with the experimental thermal analysis.

Prior to cross-sectional analysis, the surface morphology of the cobalt-coated BNi-2 powder was examined by SEM, as shown in Figure 5. The outer surface exhibits a nodular morphology characterized by hemispherical growth features and coalesced clusters, which is consistent with typical electroless cobalt deposits. Similar nodular morphologies have been widely reported for electroless cobalt and electroless Ni-based deposits, where autocatalytic surface growth leads to hemispherical cluster formation rather than true dendritic branching [27]. The cobalt layer is clearly distinguishable from the underlying powder surface, confirming complete surface coverage and strong adhesion of the coating in the as-deposited condition. To further evaluate coating uniformity and elemental distribution across the particle cross-section, the powder was embedded in bakelite and subjected to grinding and polishing.

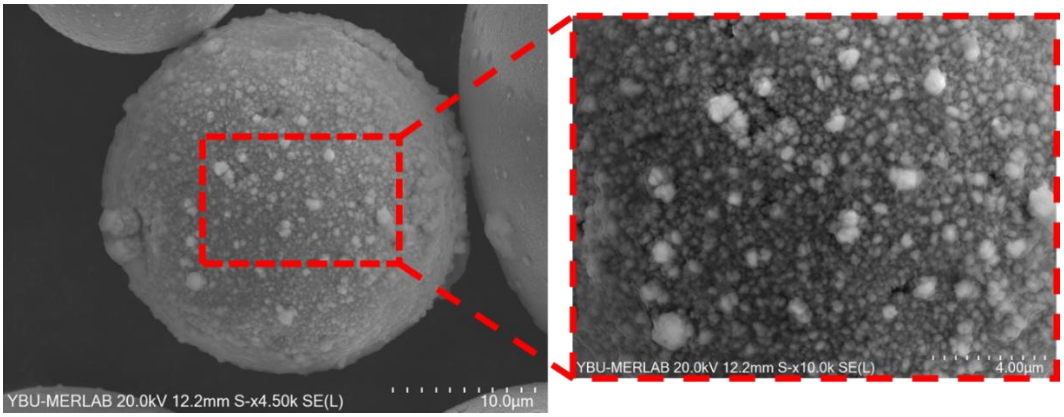

Figure 5. *SEM images of electroless cobalt-coated BNi-2 powder showing the surface morphology of the as-deposited coating. The low-magnification image (left) illustrates complete coverage of the powder surface, while the higher-magnification inset (right) highlights the nodular surface morphology with coalesced hemispherical growth features associated with autocatalytic cobalt growth*

After mounting in bakelite and completing the grinding and polishing steps, the coated powders were examined in cross-section to assess the distribution of elements across the particle interior and the deposited layer. EDS elemental mapping results are shown in Figure 6. Nickel exhibited a strong and uniform signal throughout the entire particle cross-section, consistent with the Ni-rich composition of the BNi-2 alloy. Signals corresponding to Cr, Fe, and Si were likewise detected within the interior of the particles; these elements originate from the base BNi-2 composition, and their mappings reflect their presence within the alloyed powder rather than an effect of the coating process. The cobalt map, in contrast, showed a continuous and well-defined ring along the particle periphery, demonstrating that the electroless deposition process formed a coherent cobalt-containing shell around each powder grain. The coating appeared uniform in thickness across all examined regions. It should be noted that localized discontinuities observed in certain regions of the EDS cobalt maps are attributed to mechanical damage introduced during the metallographic preparation steps, particularly grinding and polishing, rather than to intrinsic coating defects or poor interfacial bonding. Quantitative EDS analysis yielded an average composition of 82.73 wt.% Ni, 6.23 wt.% Cr, 4.42 wt.% Si, 2.85 wt.% Fe and 3.77 wt.% Co. The presence of cobalt restricted to the outer surface confirms that the coating process selectively modified the powder exterior while preserving the internal composition of the BNi-2 particles. Overall, the mapping results indicate that the cobalt layer is continuous and homogeneously distributed, verifying that the electroless plating procedure achieved uniform coverage on all analysed powder surfaces.

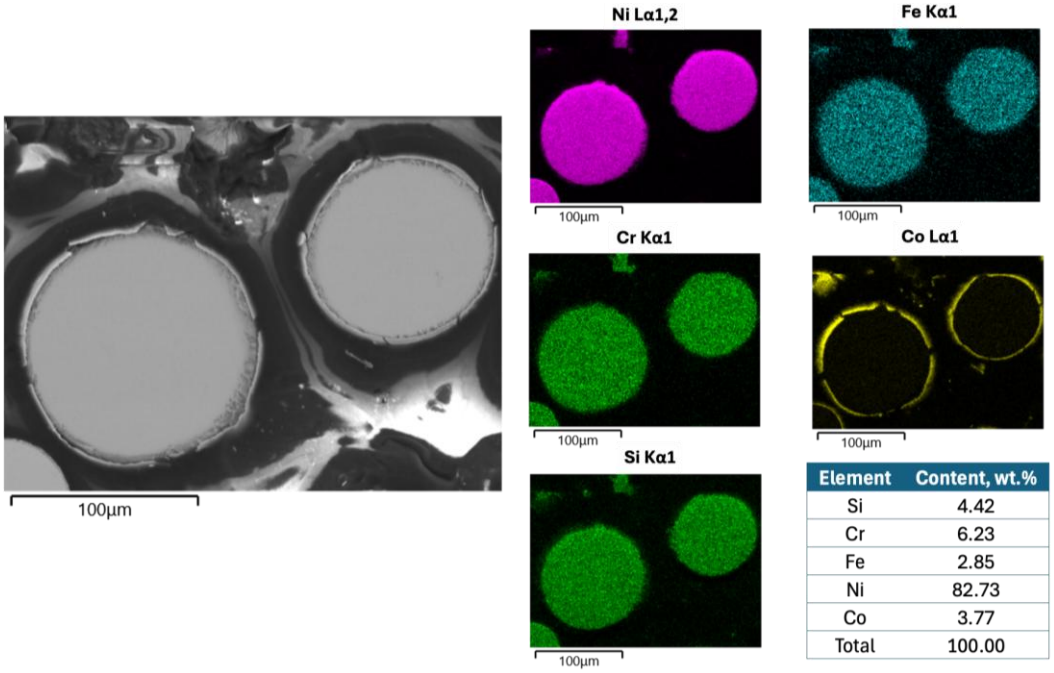

Element	Content, wt.%
Si	4.42
Cr	6.23
Fe	2.85
Ni	82.73
Co	3.77
Total	100.00

Figure 6. *Cross-sectional SEM images and corresponding EDS elemental maps of cobalt-coated BNi-2 powder, showing the distribution of Ni, Fe, Cr, Si, and Co across the particles. The Co La₁ map highlights a continuous cobalt-rich layer at the particle surface, while the quantitative EDS table confirms the overall composition of the coated powder*

To further examine the chemical state of the deposited cobalt layer, X-ray photoelectron spectroscopy (XPS) depth profiling was performed on the powder containing approximately 7 wt.% cobalt. Figure 7 shows the variation of elemental concentrations as a function of sputtering time.

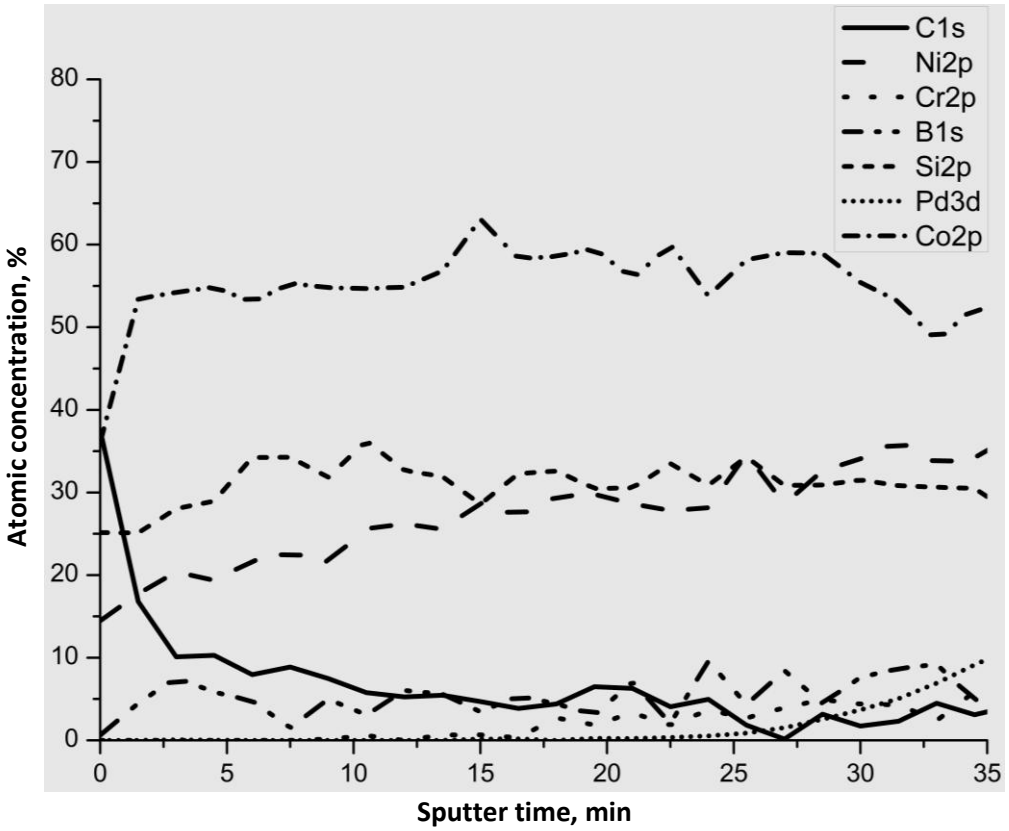

Figure 7. *XPS depth profile of the 7 wt.% Co-coated BNi-2 powder showing the variation of elemental atomic concentrations as a function of sputtering time. The profile confirms the presence of a cobalt-rich surface layer and the gradual transition to the underlying BNi-2 alloy composition*

The surface region is initially dominated by carbon contamination commonly observed in XPS measurements. With increasing sputtering time, the cobalt signal becomes dominant, confirming the presence of a cobalt-rich surface layer. The Co 2p signal remains stable throughout the sputtering depth, indicating that cobalt constitutes the main component of the coating. The presence of Ni, Cr, B and Si signals at longer sputtering times corresponds to the underlying BNi-2 substrate. The XPS results therefore support that cobalt is predominantly metallic and is confined to the powder surface.

Conclusions

- The surface preparation sequence applied to the BNi-2 powder generated catalytically active surfaces through Sn^{2+} adsorption and Pd activation, which enabled consistent initiation of the electroless cobalt deposition reaction.
- ICP-OES measurements showed that the amount of deposited cobalt varied from 1.1 to 7.0 wt.% across the selected parameter range. Higher plating temperature, higher $CoSO_4$ concentration and longer plating time each increased cobalt incorporation, while increasing NaH_2PO_2 concentration, decreased the amount of cobalt deposited.
- The regression equation obtained from the design-of-experiments analysis (Equation 1), represented the observed deposition behaviour within the investigated window and quantified the individual contributions of the coating parameters.
- Differential scanning calorimetry revealed that the solidus temperature increased from 970° C for the uncoated powder to 990 °C at the highest coating level, while the liquidus temperature decreased from 1050 to 1010 °C, resulting in a progressively narrower melting interval with increasing cobalt content.
- JMatPro simulations confirmed these thermal changes by predicting reduced MB_2 and M_3B_2 phase fractions and enhanced γ and γ’ stability as cobalt content increased.
- Cross-sectional analyses demonstrated the formation of a continuous cobalt-rich layer around the BNi-2 particles, with coating thicknesses typically between 1.5 and 2 µm, and no observable discontinuities along the particle perimeter.
- SEM-EDS mapping showed that cobalt was confined to the particle surface, forming a chemically continuous outer ring, while the internal composition remained consistent with uncoated BNi-2, indicating that the electroless process modified only the surface chemistry. This observation was further supported by XPS analysis, which confirmed the presence of a cobalt-rich surface layer on the powder particles.
- Overall, the results demonstrate that electroless cobalt deposition enables controlled and quantifiable modification of BNi-2 powder surfaces, leading to measurable changes in melting characteristics and phase stability that are relevant for future brazing applications involving high-temperature alloy systems.

Acknowledgments: *The authors gratefully acknowledge the support of Simultura Material Technologies INC. in JMatPro simulations.*

Funding: *This research received no external funding*

Data Availability Statement: *All original findings from this study are presented within the article. For additional information, interested readers may contact the corresponding author.*

Conflicts of Interest: *The authors declare that a patent application related to the subject of this study, specifically on electroless coating of brazing alloy powders, is currently under internal review prior to submission.*

Author Contributions: *Conceptualization, T.G.; methodology, T.G.; validation, T.G., Z.E. and İ.K.; formal analysis, T.G.; investigation, T.G.; resources, T.G.; writing—original draft preparation, T.G.; writing—review and editing, Z.E. and İ.K.; supervision, İ.K. All authors have read and agreed to the published version of the manuscript.*

References

[1] M. Baranowski, J. Senkara, Brazing of selected heat-resisting alloys using Ni-Pd filler metal, *Welding Technology Review* **91** (2019) 51-58. https://doi.org/10.26628/wtr.v91i10.1078

[2] K. Krystek, I. Dul, M. Wierzbińska, M. Motyka, Effect of vacuum brazing conditions of Inconel 718 superalloy sheets on microstructure and mechanical properties of joints, *Archives of Metallurgy and Materials* **69** (2024) 761-773. https://doi.org/10.24425/amm.2024.149808

[3] M. A. Penyaz, A. A. Ivannikov, O. N. Sevryukov, B. A. Kalin, Overview of nickel-based filler metals for brazing of austenitic stainless steels, *Non-Ferrous Metals* **50** (2021) 41-56. https://doi.org/10.17580/nfm.2021.01.06

[4] M. A. Arafin, M. Medraj, D. P. Turner, P. Bocher, Transient liquid phase bonding of Inconel 718 and Inconel 625 with BNi-2: Modelling and experimental investigations, *Materials Science and Engineering A* **447** (2007) 125-133. https://doi.org/10.1016/j.msea.2006.10.045

[5] A. Khorram, O. Fakhraei, M. J. Torkamany, Laser brazing of Inconel 718 and Inconel 600 with BNi-2 nickel-based filler metal, *The International Journal of Advanced Manufacturing Technology* **88** (2017) 2075-2084. https://doi.org/10.1007/s00170-016-8897-5

[6] C. Xia, M. Zhao, W. Sun, P. Liu, H. X. Li, Microstructure and properties of 3D printed Inconel 718 joint brazed with BNi-2 amorphous filler metal, *Materials Research* **22** (2018) e20180348. https://doi.org/10.1590/1980-5373-MR-2018-0348

[7] B. Binesh, M. Aghaie-Khafri, A. Fayegh, Processing of IN718/Ti-6Al-4V bimetallic joint using transient liquid phase bonding: Effect of bonding temperature on the microstructure and mechanical properties, *Philosophical Magazine* **102** (2022) 745-771. https://doi.org/10.1080/14786435.2021.2012612

[8] S. P. Kaleybar, H. Khorsand, Effect of bonding temperature on microstructure and mechanical properties of TLP-bonded Ti-6Al-4V/Inconel 718 joints using BNi2/Cu interlayer, *Journal of Advanced Joining Processes* **12** (2025) 100328. https://doi.org/10.1016/j.jajp.2025.100328

[9] G. Yan, A. Bhowmik, B. Nagarajan, X. Song, S. C. Tan, M. J. Tan, Bonding temperature effects on the wide gap transient liquid phase bonding of Inconel 718 using BNi-2 paste filler metal, *Applied Surface Science* **484** (2019) 1223-1233. https://doi.org/10.1016/j.apsusc.2019.04.070

[10] A. Ivannikov, B. Kalin, O. Sevryukov, M. Penyaz, I. V. Fedotov, V. Misnikov, M. Tarasova, Study of the Ni-Si-Be system as a base to create boron-free brazing filler metals, *Science and Technology of Welding and Joining* **23** (2017) 187-197. https://doi.org/10.1080/13621718.2017.1361668

[11] N. Siredey-Schwallller, J. Hamel-Akré, L. Peltier, A. Hazotte, P. Bocher, Solidificaton sequence of Ni-Si-Cr 3 wt% B brazing alloys, *Welding in the World* **61** (2017) 1253-1265. https://doi.org/10.1007/s40194-017-0503-4

[12] S. K. Tung, L. C. Lim, M. O. Lai, Solidification phenomena in nickel base brazes containing boron and silicon, *Scripta Materialia* **34** (1996) 729-734. https://doi.org/10.1016/1359-6462(95)00577-3

[13] L. Hardwick, P. Rodgers, E. Pickering, R. Goodall, Development of a Novel Ni-Based Multi-principal Element Alloy Filler Metal, Using an Alternative Melting Point Depressant. *Metallurgical and Materials Transactions A* **52** (2021) 2534-2548, https://doi.org/10.1007/s11661-021-06246-0

[14] K. Bobzin, H. Heinemann, M. Erck, Microstructural modification by redesigning the chemical composition of Ni 620 filler metal, *Advanced Engineering Materials* **25** (2023) 2300318. https://doi.org/10.1002/adem.202300318
[15] M. Pouranvari, A. Ekrami, A. H. Kokabi. Role of base-metal composition in isothermal solidification during diffusion brazing of nickel-based superalloys, *Science and Technology of Welding and Joining* **23** (2018) 13-18. https://doi.org/10.1080/13621718.2017.1321335
[16] X. Yang, L. Xu, Y. Gao, Y. Liang, X. Zhang, Y. Yang, Performance of the GH4169 joint using a novel Ni-based brazing filler metal designed via phase diagram calculations, *Metals* **14** (2024) 1274. https://doi.org/10.3390/met14111274
[17] J. S. C. Jang, H. P. Shih, Study of the nano-structured nickel-based brazing filler synthesized by mechanical alloying, *Materials Chemistry and Physics* **70** (2001) 217-222. https://doi.org/10.1016/S0254-0584(00)00507-1 .
[18] J. Huang, Z. Chen, Method for electroless nickel plating on the surface of $CaCO_3$ powders, *RSC Advances* **7** (2017) 25622-25629. https://doi.org/10.1039/C7RA03110F
[19] A. Kilicarslan, F. Toptan, H. Koralay, Electroless nickel-phosphorus coating on boron carbide particles, *Journal of Materials Engineering and Performance* **21** (2012) 966-973. https://doi.org/10.1007/s11665-011-0021-0
[20] J. Sudagar, J. Lian, W. Sha, Electroless nickel, alloy, composite and nano coatings - A critical review, Journal of Alloys and Compounds 571 (2013) 183-204. https://doi.org/10.1016/j.jallcom.2013.03.107
[21] E. Hosseini, M. Amirjan, N. Parvin, Preparation and characterization of nickel-based brazing powder: Cobalt and chromium addition effects, *Powder Metallurgy* **66** (2023) 64-76. https://doi.org/10.1080/00325899.2022.2073013
[22] T. Göynük, Z. Esen, İ. Karakaya, Enhancement of brazing performance of Inconel 718 by electroless cobalt coated nickel-based brazing alloys, *Journal of Materials Research and Technology* **39** (2025) 4705-4713. https://doi.org/10.1016/j.jmrt.2025.10.110
[23] T. Göynük, İ. Karakaya, G. Can, M. Yücel, Patent application filed *Production of composite nickel-based vacuum hard soldering alloy powder by electroless plating*, Roketsan Roket Sanayi ve Ticaret A.Ş., TR2025/013192, 2025. https://portal.turkpatent.gov.tr/anonim/arastirma/patent/sonuc/dosya?patentAppNo=2025/013192&documentsTpye=all (in Turkish)
[24] L. Guo, X. J. Zhao, L. R. Xiao, C. R. Tang, W. Y. Zhang, X. X. Tu, X. Z. Liu, Y. C. Nie, Kinetic study of electroless cobalt deposition on WC particles, *Journal of Alloys and Compounds* **750** (2018) 774-780. https://doi.org/10.1016/j.jallcom.2018.04.064
[25] Minitab LLC, Minitab® Statistical Software, Pennsylvania, USA, https://www.minitab.com/en-us/.
[26] Sente Software Ltd., JMatPro® Software, Surrey, United Kingdom, https://www.sentesoftware.co.uk.
[27] M.-A. Chen, N. Cheng, Y.-C. Ou, J.-M. Li, Corrosion performance of electroless Ni-P on polymer coating of MAO coated AZ31 magnesium alloy, *Surface and Coatings Technology* **232** (2013) 726-733. https://doi.org/10.1016/j.surfcoat.2013.06.087